Commun. Theor. Phys. **63** (2015) 619–624 Vol. 63, No. 5, May 1, 2015

Molecular Dynamics Studies on Ballistic Thermal Resistance of Graphene Nano-Junctions*

YAO Wen-Jun (姚文俊) and CAO Bing-Yang (曹炳阳)†

Key Laboratory for Thermal Science and Power Engineering of Ministry of Education, Department of Engineering Mechanics, Tsinghua University, Beijing 100084, China

(Received December 1, 2014; revised manuscript received January 30, 2015)

Abstract *Ballistic thermal resistance of graphene nano-junctions is investigated using non-equilibrium molecular dynamics simulation. The simulation system is consisted of two symmetrical trapezoidal or rectangular graphene nano-ribbons (GNRs) and a connecting nanoscale constriction in between. From the simulated temperature profile, a big temperature jump resulted from the constriction is found, which is proportional to the heat current and corresponds to a local ballistic thermal resistance. Fixing the constriction width and the length of GNRs, this ballistic thermal resistance is independent of the width of the GNRs bottom layer, i.e., the convex angle. But interestingly, this thermal resistance has obvious size effect. It is inversely proportional to the constriction width and will disappear with the constriction being wider. Moreover, based on the phonon dynamics theory, a theoretical model of the ballistic thermal resistance in two-dimensional nano-systems is developed, which gives a good explanation on microcosmic level and agrees well with the simulation result quantitatively and qualitatively.*

PACS numbers: 65.80.+n, 61.48.De, 63.20.kp, 31.15.xv
Key words: graphene, ballistic resistance, molecular dynamics simulation

1 Introduction

Since graphene was first exfoliated from graphite in 2004,[1] much attention has been attracted for its perfect two-dimensional (2D) structure. Similar to other carbon allotropes, i.e., carbon nanotubes[2] and diamond,[3] very high thermal conductivity has been measured for graphene: 1450–5150 W/(m·K) for a suspended single-layer graphene,[4−8] 1250–2800 W/(m·K) for a multilayer graphene[7−10] and about 600 W/(m·K) for a substrate-supported monolayer graphene.[6,10−11] Excellent thermal properties of graphene make it one of the most promising materials in solving heat dissipation problems such as those in nanoelectronics.[9,12−15] But nanoelectronic devices are of complex shapes in real situation and structural configuration is an important but less-studied factor impacting the thermal properties of graphene, which can affect the lifetime and reliability of the graphene-based nano-devices seriously, especially when the characteristic dimension is less than the phonon mean free path of graphene (about 775 nm at room temperature[5]). Xu *et al.* investigated the thermal transport properties of various graphene junctions and quantum dots using Green's-function method and found that the thermal conductance is substantially limited by the narrowest part of the system.[16] Thus, understanding the carrier transport of graphene with specific structure is of great scientific and technological importance.

Besides, considering both high electron mobility and high thermal conductivity of graphene, many scholars studied and demonstrated that the thermoelectric efficiency can be significantly improved[17] by suppressing the thermal conductance of graphene with nanostructuring techniques such as edge roughness[18−19] and defect engineering.[20−21] Cooper *et al.* and Prasher *et al.*[22−25] found that the geometrical constriction can introduce a ballistic thermal resistance in the ballistic regime where the characteristic dimension of the constriction is much smaller than the phonon mean free path, which weakens the thermal transport dramatically. And they modeled this ballistic resistance of three-dimensional (3D) systems accounting for microscale effects. Similarly, if we can efficiently reduce the thermal conductance of graphene by constructing such specific structure and introducing the ballistic thermal resistance, structural configuration maybe suggest an alternative way to improve the thermoelectric figure of merit in graphene nanostructures.

In this work, we hence construct the system consisting of two symmetrical trapezoidal or rectangular graphene nano-ribbons (GNRs) and a connecting nanoscale constriction in between and investigate the heat conduction of this simulation system. From the temperature profile, a big temperature jump is found near the constriction,

*Supported by the National Natural Science Foundation of China under Grant Nos. 51322603, 51136001, 51356001, Science Fund for Creative Research Groups (No. 51321002), the Program for New Century Excellent Talents in University, Tsinghua University Initiative Scientific Research Program, the Tsinghua National Laboratory for Information Science and Technology of China

†Corresponding author, E-mail: caoby@tsinghua.edu.cn

which creates a local ballistic resistance. Moreover, we study the effect of the heat current, convex angle and constriction width on this thermal resistance and develop a ballistic thermal resistance model of 2D system, based on the phonon dynamics theory, to predict the ballistic resistance of nanoscale graphene junctions.

2 Molecular Dynamics Simulations

The simulation system is consisted of two symmetrical trapezoidal or rectangular GNRs and a connecting nanoscale constriction in between. The system with trapezoidal GNRs are shown in Fig. 1, where the system length L fixed for all simulation cases is 20.6 nm and the convex angle ϕ of the GNR is 60°. The convex angle ranges from 0° to 180° for trapezoidal GNRs and equals 180° for rectangular GNRs. The top sketch in Fig. 1 depicts the detailed structure of the connecting part between two GNRs, where w is the constriction width. This part is the narrowest part of the system, so that heat is constricted to flow only through such small area in contact. What is more, the width of this part is from 0.29 nm to 4.18 nm, so we call this part as nanoscale constriction and call this system as graphene nano-junctions.

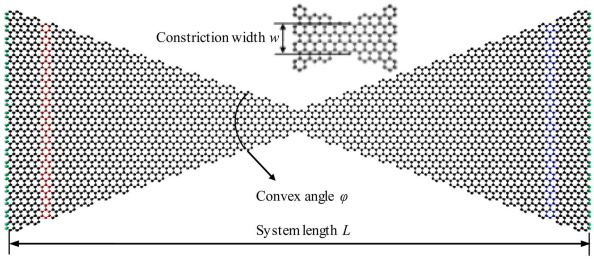

Fig. 1 (Color online) Schematic of the simulation system including a high-temperature slab (red) and a low-temperature slab (blue) with fixed boundaries (green). The top sketch depicts the detailed structure of the constriction.

Fixed boundary conditions are used at GNRs bottom layers, i.e., the green atoms in Fig. 1, to prevent spurious global rotation and translation of the system. Here, we employ the non-equilibrium molecular dynamics (NEMD) method[26−30] and the heat current from the high temperature slab (the red part) to the low temperature slab (the blue part) is obtained by the velocity exchange method developed by Müller.[31] According to this method, the heat current J can be described as

$$J = \frac{\sum_{\text{transfers}} (m/2)(v_h^2 - v_c^2)}{t}, \tag{1}$$

where m is the atomic mass of carbon, v_h is the velocity of the hottest atom in the low temperature slab, v_c is the velocity of the coldest atom in the high temperature slab and t is the statistical time. Total energy and momentum of the system are conserved during the velocity-exchange, while the system temperature is kept at 300 K using the Nosé–Hoover thermostat method.[32] Some atoms between the velocity-exchange slabs and the fixed boundaries are left to reduce the boundary temperature jump.[33]

In the molecular dynamics (MD) simulation, the bond-order potential presented by Brenner[34] is used to describe the carbon-carbon bonding interactions,

$$E = \sum_i \sum_{j(>i)} f(r_{ij})[V_R(r_{ij}) - b_{ij} V_A(r_{ij})], \tag{2}$$

where E_b is the total potential energy, $V_R(r)$ and $V_A(r)$ are, respectively, repulsive and attractive interactions, $f(r)$ is the truncation function that explicitly restricts the potential to nearest neighbors and b_{ij} is the many-body interaction parameter. The motion equations of atoms are integrated by a leap-frog scheme with a fixed time step of 0.5 fs. Each simulation case runs for 1 ns to reach a steady state, and then for 1.5 ns to average the temperature profile and heat current over time. During the simulation, we divide the system into 50 slabs along the length direction, and the local instantaneous temperature for each slab, according to the energy equipartition theorem, is defined through the averaged kinetic energy as:

$$T_i = \frac{2}{3N_i k_B} \sum_{j=1}^{N_i} \frac{P_j^2}{2m}, \tag{3}$$

where N_i is the atom number of i-th slab, k_B is the Boltzmann constant and P_j is the momentum of the j-th atom.

3 Results and Discussions

We employ the velocity exchange method developed by Müller[31] to generate the heat current, but in this paper, we do not set the velocity exchange interval to a constant value. Specifically, we obtain the heat current through such an improved process: compare the actual heat current with the preset value during the simulation, if the former is smaller than the latter, exchange the velocity of the coldest atom in the high temperature slab and that of the hottest atom in the low temperature slab. In this way, we can adjust the frequency of the velocity-exchange in real time and achieve the preset heat current accurately.

3.1 *Effect of the Heat Current*

Figure 2 shows three typical temperature profiles of the system under different heat currents. As mentioned before, each system is consisted of two symmetrical GNRs and a connecting constriction. Combined with the system structure, we can see that the temperature profile is also symmetrical. Although the width of GNR is gradually decreasing or increasing, that is to say, the heat flux density is changing, the temperature profile still shows approximate linear characteristics, because of the effect of thermal conductivity on the width of GNR.[35−37] What is more, a big temperature jump is found in the middle, which indicates that energy is seriously blocked when passing

through the nanoscale constriction and thus an additional thermal resistance is introduced. Considering the characteristic dimension of the constriction is much smaller than the phonon mean free path of graphene (about 775 nm at room temperature[5]), the thermal transport across the constriction typically falls in a ballistic regime, thus, this additional thermal reisistance is a ballistic thermal resistance.

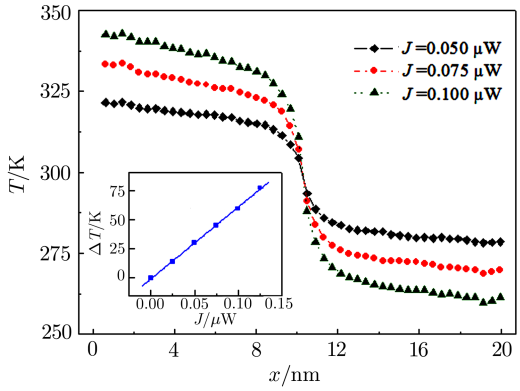

Fig. 2 Three typical temperature profiles of the system with a constriction width of 0.72 nm, a convex angle of 60°, under different heat currents. The inset shows the temperature jump versus heat current.

Based on the definition of the interfacial thermal resistance, i.e., Kappitza resistance,[38] the ballistic thermal resistance at the connecting constriction can be defined as

$$R = \frac{\Delta T}{J}. \tag{4}$$

Here, by fitting the temperature distributions between the nanoscale constriction and the velocity-exchange slabs, we define the temperature difference at the constriction between the two fitting lines as the temperature jump ΔT, and J is the associated heat current across the constriction. The inset in Fig. 2 shows the dependence of the temperature jump on the heat current. As shown, with the heat current increasing, the temperature jump approximately increases linearly, which indicates that the ballistic resistance of constriction is an intrinsic property of the system and independent of the heat current. Thus, to reduce the error, the thermal resistance R can be calculated by fitting the curve between the temperature jump and the heat current passing through the origin.

3.2 *Effect of the Convex Angle*

To investigate the effect of the convex angle, we fix the constriction width of GNRs at 1.15 nm and only convex angle $\phi = 38.2°$, 60°, 81.7°, 120°, 180° are chosen in order to reduce the effect of edge roughness. Meanwhile, as Fig. 3 shows, because the thermal resistance of constriction is a local value which relates only to phonons passing through the constriction, the resistance is independent of the system length L, so we set the length $L = 20.6$ nm for all simulation cases for convenience. When the convex angle is 60° and 180°, the system contains two GNRs with edge chirality of armchair, and when convex angle is 120°, the edge chirality of GNRs is zigzag. The calculated temperature profiles of the above five systems under same heat current are shown in Fig. 4.

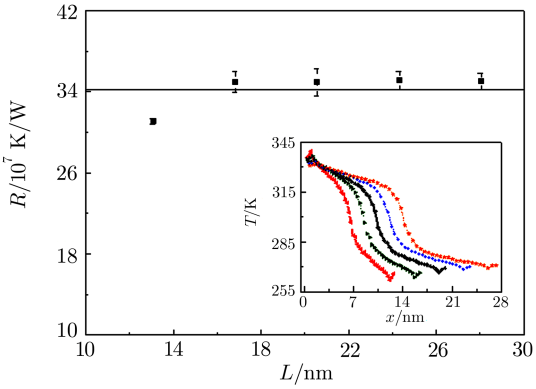

Fig. 3 Thermal resistance of constriction as a function of the system length. The line represents the average of five values. And the inset shows temperature profiles of the system, from left to right, with a system length of 13.1 nm, 16.8 nm, 20.6 nm, 24.3 nm, and 28.1 nm, respectively, under the heat current $J = 0.100$ μW.

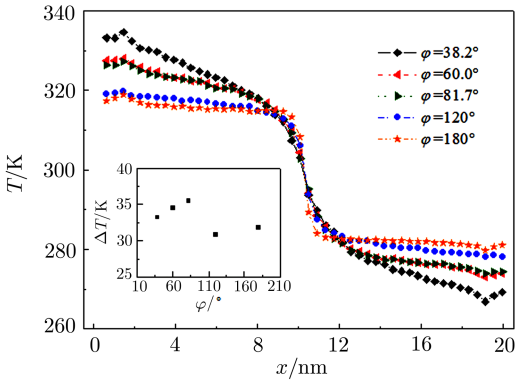

Fig. 4 Temperature profiles of the system with a constriction width of 1.15 nm, a convex angle of 38.2°, 60°, 81.7°, 120°, and 180°, respectively, under the heat current $J = 0.100$ μW. And the inset shows the temperature jump versus convex angle.

In Fig. 4, as the convex angle increasing, the maximum temperature difference of the system is reduced from 68 K to 40 K, which can be analyzed from the causes of the linear temperature profile and the temperature jump at the nanoscale constriction. Fixing the constriction width and the length of GNRs, as the convex angle increasing, the width of each GNR slab being wider and the heat flux density being smaller under the same heat current. So we can see from Fig. 4, the linear temperature distributions of the system with bigger convex angle is more gentle than that of smaller one. Yet, as shown in the inset of Fig. 4, despite the temperature distribution in the linear region

is different, the temperature jump at the constriction is almost equal for different convex angle.

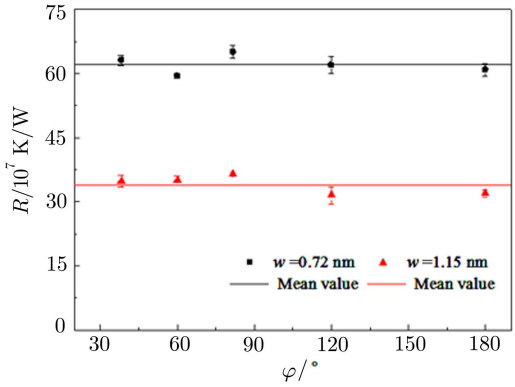

Fig. 5 Thermal resistance of constriction as a function of convex angle for the system with a constriction width of 0.72 nm and 1.15 nm, respectively. The lines represent the average of five values of the two systems, respectively.

Figure 5 shows the dependence of the ballistic thermal resistance on the convex angle. In accordance with above conclusion, the thermal resistance is almost equal for different convex angle, which indicates that the ballistic thermal resistance is independent of the convex angle and insensitive to the detailed structure of GNR. But we can also see that for different constriction width, with a fixed convex angle, the thermal resistance varies with the constriction width. When the width is 0.72 nm, the thermal resistance is around 3.4×10^8 K/W. But when the width is 1.15 nm, that is around 6.2×10^8 K/W. This thermal transport behavior is distinctly different from that of the bulk material, which is independent of the size, and indicates that the ballistic thermal resistance of graphene nano-junctions has obvious size effect.

3.3 *Effect of the Constriction Width*

To study the effect of the constriction width on the heat conduction, the systems with the atom number at the constriction are 2, 4, 6, 8, 10, 20, i.e., the width of the constriction are 0.29 nm, 0.72 nm, 1.15 nm, 1.58 nm, 2.02 nm, 4.18 nm are simulated. The calculated results are shown in Fig. 6.

Figure 6 shows the ballistic thermal resistance as a function of constriction width as the convex angle varies from 38.2° to 180°. As shown, various sized constrictions create large ballistic resistance, which are on the order of 10^7–10^9 K/W. And as mentioned before, the ballistic resistance is independent of the convex angle but has obvious size effect. With the constriction width increasing, which means the strength of the constriction weakening, the ballistic resistance decreases quickly from 1.45×10^9 K/W to 5.64×10^7 K/W and it is almost inversely proportional to the width of constriction.

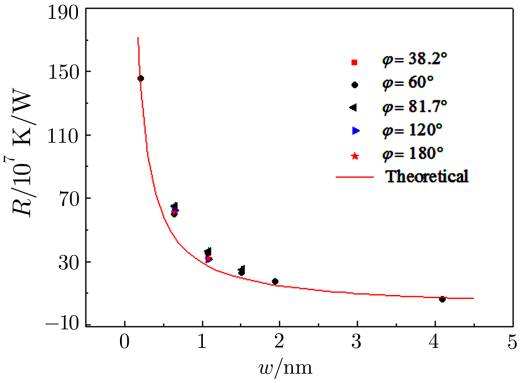

Fig. 6 Ballictic thermal resistance of constriction as a function of constriction width. The curve is the theoretical prediction given by Eq. (7).

3.4 *Phonon Analyses*

In this paper, the constriction width ranges from 0.29 nm to 4.18 nm, which is much smaller than the phonon mean free path of graphene (about 775 nm at room temperature[5]). Thus, the diffusive resistance can be ignored and the thermal resistance at the constriction is dominated by the ballistic resistance created by ballistic phonon transport. Similar to 3D material,[22–25] the heat current for 2D grephene in the ballistic regime can be described as

$$J = \frac{2A}{\pi}\left[\sum_3 \int_{\omega=0}^{\omega_m}\int_{\theta=0}^{\pi/2} \frac{\hbar\omega}{\exp(\hbar\omega/k_BT)-1} D(\omega)v_g(\omega)\tau(\omega,\theta)\,\mathrm{d}\theta\,\mathrm{d}\omega\right], \tag{5}$$

where ω is the frequency of phonons, ω_m is the maximum frequency, $\hbar$ is the reduced Planck constant, $1/(\exp(\hbar\omega/k_BT)-1)$ is the occupation of phonons given by the Bose–Einstein distribution correspond to the local equilibrium temperature T, D (ω) is the phonon density of states, $v_g(\omega)$ is the phonon group velocity, $\tau(\omega,\theta) = \cos\theta$ is the transmissivity of phonons, i.e., the ratio of the projected area in the direction of the incident wave and the real area of the constriction[24–25] and θ is the direction angle. Assume the phonon group velocity (v_g) is independent of the phonon frequency and phonon modes, Eq. (5) is simplified to

$$J = \frac{2w\delta v_g U}{\pi}, \tag{6}$$

where $\delta = 0.335$ nm is the thickness of the graphene sheet,[15,39] U is the interval energy per unit volume. Then, the ballistic thermal resistance can be given as

$$R_b = \frac{\Delta T}{J} = \frac{\pi}{2w\delta c_v v_g}, \tag{7}$$

where c_v is the heat capacity per unit volume. Equa-

tion (7) indicates that the ballistic resistance is proportional to the reciprocal of the constriction width, which is consistent with the conclusion derived from MD results. In the classical MD simulation, without the quantum correction, the heat capacity per unit volume is $c_v = 3Nk_B/V$, in which N and V are the atom number and the volume of the system, respectively. And the effective phonon group velocity v_g is calculated from the equation $1/v_g^3 = (1/v_l^3 + 1/v_t^3 + 1/v_z^3)/3$. Here, the group velocity of three acoustic phonon branches $v_l = 21.04$ km/s, $v_t = 14.9$ km/s and $v_z = 2.5$ km/s[40] are taken and then we substitute c_v and v_g into Eq. (7), the dependence of the ballistic resistance on the constriction width is obtained, shown in Fig. 6, which reveals that the ballistic thermal resistance is inversely proportional to the constriction width, and the predicted values of this model agree well with the simulation results.

4 Conclusions

The field of graphene is now rapidly extended from science lab to engineering workshop, which requires more comprehensive understanding of the characteristic of carrier transport in graphene with specific structure and the effect of the structure configuration on the thermal transport properties. In this paper, we construct various graphene junctions, each contains two symmetrical trapezoidal or rectangular GNRs and a connecting constriction of few nanometers in size, and simulate the heat conduction process using NEMD method. Heat current is generated by exchanging velocity vector of atoms. By fitting the linear temperature profiles between the constriction and the velocity-exchange slabs, a big temperature jump between the two fitting lines at the constriction is extracted, which corresponds to a ballistic thermal resistance. What is more, we study the effect of the heat current, convex angle and constriction width on this ballistic resistance. We find that the ballistic resistance of constriction is independent of the heat current and convex angle, which indicates that it is an intrinsic property of the system and insensitive to the detailed structure of GNR. But interestingly, the ballistic thermal resistance has obvious size effect. It is inversely proportional to the constriction width and will disappear with the constriction being wider. Moreover, based on the phonon dynamics theory, we develop a ballistic thermal resistance model for 2D material, which gives a good explanation on the microcosmic level. And the model prediction agrees well with the simulation result, which suggests that the thermal transport across the junction is truly in the ballistic regime and the heat transport of graphene can be predicted or controlled by the structural configuration method.

Abbreviations

2D: two-dimensional; MD: molecular dynamics; GNR: graphene nanoribbon; NEMD: nonequilibrium molecular dynamics; 3D: three-dimensional.

References

[1] K.S. Novoselov, A.K. Geim, S.V. Morozov, D. Jiang, Y. Zhang, S.V. Dubonos, I.V. Grigorieva, and A.A. Firsov, Science **306** (2004) 666.

[2] M. Fujii, X. Zhang, H. Xie, H. Ago, K. Takahashi, T. Ikuta, H. Abe, and T. Shimizu, Phys. Rev. Lett. **95** (2005) 065502.

[3] G.A. Slack, J. Appl. Phys. **35** (1964) 3460.

[4] A.A. Balandin, S. Ghosh, W. Bao, I. Calizo, D. Teweldebrhan, F. Miao, and C.N. Lau, Nano Lett. **8** (2008) 902.

[5] S. Ghosh, I. Calizo, D. Teweldebrhan, E.P. Pokatilov, D.L. Nika, A.A. Balandin, W. Bao, F. Miao, and C.N. Lau, Appl. Phys. Lett. **92** (2008) 151911.

[6] W. Cai, A.L. Moore, Y. Zhu, X. Li, S. Chen, L. Shi, and R.S. Ruoff, Nano Lett. **10** (2010) 1645.

[7] A.A. Balandin, Nature Mater. **10** (2011) 569.

[8] S. Chen, Q. Wu, C. Mishra, J. Kang, H. Zhang, H. Zhang, K. Cho, W. Cai, A.A. Balandin, and R.S. Ruoff, Nature Mater. **11** (2012) 203.

[9] S. Ghosh, W. Bao, D.L. Nike, S. Subrina, E.P. Pokatilov, C.N. Lau, and A.A. Balandin, Nature Mater. **9** (2010) 555.

[10] Z. Wang, R. Xie, C.T. Bui, D. Liu, X. Ni, B. Li, and J.T.L. Thong, Nano Lett. **11** (2010) 113.

[11] J.H. Seol, I. Jo, A.L. Moore, L. Lindsay, Z.H. Aitken, M.T. Pettes, X. Li, Z. Yao, R. Huang, D. Brido, N. Mingo, R.S. Ruoff, and L. Shi, Science **328** (2010) 213.

[12] A.K. Geim and P. Kim, Sci. Am. **298** (2008) 90.

[13] C. Soldano, A. Mahmood, and E. Dujardin, Carbon **48** (2010) 2127.

[14] P.Y. Huang, C.S. Ruiz-Vargas, A.M. Zande, W.S. Whitney, M.P. Levendorf, J.W. Kevek, S. Garg, J.S. Alden, C.J. Hustedt, Y. Zhu, J. Park, P.L. McEuen, and D.A. Muller, Nature (London) **469** (2011) 389.

[15] E. Pop, V. Varshney, and A.K. Roy, MRS Bull. **37** (2012) 1273.

[16] Y. Xu, X. Chen, J.S. Wang, B.L. Gu, and W. Duan, Phys. Rev. B **81** (2010) 195425.

[17] V.H. Nguyen, M.C. Nguyen, H. Nguyen, J. Saint-Martin, and P. Dollfus, Appl. Phys. Lett. **105** (2014) 133105.

[18] H. Sevinçli and G. Cuniberti, Phys. Rev. B **81** (2010) 113401.

[19] H. Karamitaheri1, N. Neophytou, M. Pourfath, R. Faez, and H. Kosina, J. Appl. Phys. **111** (2012) 054501.

[20] H. Karamitaheri, M. Pourfath, R. Faez, and H. Kosina, J. Appl. Phys. **110** (2011) 054506.

[21] J. Haskins, A. Kinaci, C. Sevik, H. Sevincli, G. Cuniberti, and T. Cagin, ACS Nano **5** (2011) 3779.

[22] M.G. Cooper, B.B. Mikic, and M.M. Yovanovish, Int. J. Heat Mass Transfer **12** (1969) 279.
[23] R. Prasher, Nano Lett. **5** (2005) 2155.
[24] R. Prasher, Phys. Rev. B **74** (2006) 165413.
[25] R. Prasher, T. Tong, and A. Majumdar, Appl. Phys. Lett. **91** (2007) 143119.
[26] Y.W. Li and B.Y. Cao, J. Chem. Phys. **133** (2010) 024106.
[27] G.J. Hu and B.Y. Cao, J. Appl. Phys. **114** (2013) 224308.
[28] W.R. Zhong, M.M. Yang, M.P. Zhang, and B.Q. Ai, Commun. Theor. Phys. **60** (2013) 353.
[29] W.J. Yao and B.Y. Cao, Chin. Sci. Bull. **59** (2014) 3495.
[30] Z.Q. Ye, B.Y. Cao, and Z.Y. Guo, Carbon **66** (2014) 567.
[31] F. Müller-Plathe, J. Chem. Phys. **106** (1997) 6082.
[32] W.G. Hoover, Phys. Rev. A **31** (1985) 1695.
[33] J.W. Jiang, J. Chen, J.S. Wang, and B. Li, Phys. Rev. B **80** (2009) 052301.
[34] D.W. Brenner, Phys. Rev. B **42** (1990) 9458.
[35] Y. Xu, X. Chen, B.L. Gu, and W. Duan, Appl. Phys. Lett. **95** (2009) 233116.
[36] Z. Guo, D. Zhang, and X.G. Gong, Appl. Phys. Lett. **95** (2009) 163103.
[37] W.J. Evans, L. Hu, and P. Keblinski, Appl. Phys. Lett. **96** (2010) 203112.
[38] E.T. Swartz and R.O. Pohl, Rev. Mod. Phys. **61** (1989) 605.
[39] J. Hu, X. Ruan, and Y.P. Chen, Nano Lett. **9** (2009) 2730.
[40] Z.Q. Ye, B.Y. Cao, and Z.Y. Guo, Acta Phys. Sin. **63** (2014) 154704.